In-Plane Propagation of Light in Transition Metal Dichalcogenide Monolayers: Optical Selection Rules

G. Wang,[1] C. Robert,[1] M. M. Glazov,[2] F. Cadiz,[1] E. Courtade,[1] T. Amand,[1] D. Lagarde,[1] T. Taniguchi,[3] K. Watanabe,[3] B. Urbaszek,[1] and X. Marie[1]

[1]*Université de Toulouse, INSA-CNRS-UPS, LPCNO, 135 Avenue de Rangueil, 31077 Toulouse, France*

[2]*Ioffe Institute, 26 Polytechnicheskaya, 194021 St. Petersburg, Russia*

[3]*National Institute for Materials Science, Tsukuba, Ibaraki 305-0044, Japan*

(Received 16 March 2017; published 26 July 2017)

The optical selection rules for interband transitions in WSe_2, WS_2, and $MoSe_2$ transition metal dichalcogenide monolayers are investigated by polarization-resolved photoluminescence experiments with a signal collection from the sample edge. These measurements reveal a strong polarization dependence of the emission lines. We see clear signatures of the emitted light with the electric field oriented perpendicular to the monolayer plane, corresponding to an interband optical transition forbidden at normal incidence used in standard optical spectroscopy measurements. The experimental results are in agreement with the optical selection rules deduced from group theory analysis, highlighting the key role played by the different symmetries of the conduction and valence bands split by the spin-orbit interaction. These studies yield a direct determination of the bright-dark exciton splitting, for which we measure 40 ± 1 meV and 55 ± 2 meV in WSe_2 and WS_2 monolayer, respectively.

DOI: 10.1103/PhysRevLett.119.047401

Two-dimensional (2D) crystals of transition metal dichalcogenides such as MX_2 (M = Mo, W; X = S, Se, Te) are promising atomically flat semiconductors for applications in electronics and optoelectronics [1–5]. The optical properties of transition metal dichalcogenide (TMD) monolayers (MLs) are governed by very robust excitons with binding energy of the order of 500 meV [6–12]. The interplay between inversion symmetry breaking and strong spin-orbit coupling in these MLs also yields unique spin or valley properties [13–19]. Because of the 2D character of the layered materials, the band-to-band transitions are predicted to be anisotropic for light propagating parallel to the plane of the ML. The insights gained from these types of experiments in III-V semiconductor quantum wells [20,21] were crucial for designing optoelectronic devices. For 2D materials based on TMDs the light polarized perpendicular to the ML (z direction) should involve transitions with energies different from the transitions observed for in-plane polarized light [22,23]. So far, however, optical spectroscopy measurements in TMD MLs have only been made for normal incidence for which the z polarization is not accessible. Also, optical experiments performed for light propagating parallel to the ML should bring precious information on the detailed band structure of these 2D materials. In particular, it allows for a straightforward determination of the energy difference between bright and dark excitons, for which a direct measurement is still lacking [24–28].

In this Letter we present the first measurements of the luminescence properties of TMD MLs for light propagating along the plane of the layer. We measure the polarization-dependent emission properties of different TMD MLs for this in-plane optical excitation and detection geometry. For WSe_2 and WS_2 MLs, a new luminescence line emerges for the polarization perpendicular to the 2D material plane, corresponding to a z-dipole transition. This transition is forbidden at normal incidence in linear optical spectroscopy because the electromagnetic field is transverse. Our measurements yield a direct determination of the bright-dark exciton splitting, in agreement with the selection rules deduced from group theory. We find 40 and 55 meV in WSe_2 and WS_2 MLs, respectively. For $MoSe_2$ ML, no signature of the dark state is evidenced as a consequence of the very low population of the dark exciton states that lie at higher energy compared to the bright ones [23,29–31].

We have investigated MX_2 MLs encapsulated in hexagonal boron nitride (h-BN) and transferred onto an $SiO_2(90\ \text{nm})/\text{Si}$ substrate; see schematics in Figs. 1(a) and 1(b). It was shown recently that encapsulation of MX_2 ML in high-quality h-BN results in very high-quality samples where surface protection and substrate flatness yield very small photoluminescence (PL) or reflectivity linewidths, in the range 2–5 meV at low temperature [32–35]. In the present investigation the narrow exciton lines allow us to identify clearly transitions involving different bands for different polarizations of the light propagating in the ML plane. These van der Waals heterostructures are obtained by mechanical exfoliation of bulk MX_2 (from 2D Semiconductors, USA) and h-BN crystals [36], as in Ref. [34]. The typical thickness of the h-BN layers is $\sim$10 nm and the in-plane size of the MX_2 ML is $\sim 10 \times 10\ \mu\text{m}^2$. The samples are held on a cold finger in a closed-cycle cryostat. Two configurations for the microscope objective inside the cryostat are used for the excitation and collection of PL along or perpendicular to

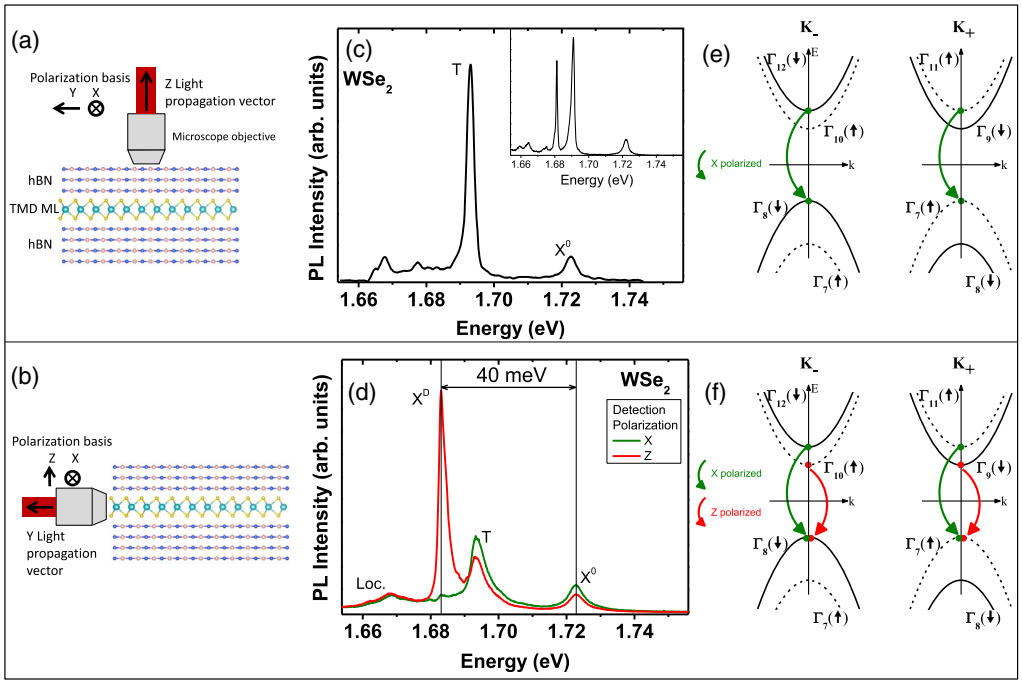

FIG. 1. Schematics of the excitation or detection geometry of the PL for (a) light propagating perpendicular to the ML plane, detection of the PL from the top of the sample, and (b) light propagating parallel to the ML plane, detection of the PL from the edge of the sample. (c) Detection of the PL from the top of the sample with a NA = 0.6 objective. The PL spectrum of h-BN/WSe_2 ML/h-BN at $T = 13$ K; the polarization of the excitation or detected light is in the ML plane (x direction). The inset shows the PL spectrum measured with a higher NA objective (NA = 0.82). (d) Detection of the PL from the edge of the sample. The PL spectrum of h-BN/WSe_2 ML/h-BN at $T = 13$ K; the polarization of the detected light is in the ML plane (x direction), green line, or perpendicular to it (z direction), red line. (e) Sketch of the band structure of WSe_2 ML. The bands are labeled in each valley by the corresponding irreducible spinor representations with arrows in parentheses indicating the dominant electron spin orientation. The green arrows show the transitions optically active for the x-polarized light; (f) the green and red arrows show the transitions optically active for x-polarized and z-polarized light, respectively (light propagating parallel to the ML plane).

the ML plane, Figs. 1(a) and 1(b). Attocube X-Y-Z piezomotors allow for positioning with nm resolution of the ML with respect to the microscope objective (numerical aperture NA = 0.82 unless otherwise stated) used for excitation and collection of luminescence. The ML is excited by a continuous wave green laser (2.33 eV). For WSe_2 and $MoSe_2$ MLs similar results have been obtained with He-Ne laser excitation (1.96 eV). The laser average power is about 50 μW. The excitation laser and detection spot diameter is $\sim$1 μm. The PL signal is dispersed in a spectrometer and detected with a Si-CCD camera [37,38].

Figure 1(c) presents the PL spectrum at $T = 13$ K of the WSe_2 ML in the standard configuration, i.e., propagation of light perpendicular to the ML. We observe clearly the peaks corresponding to the recombination of neutral exciton X^0 (1.722 eV), a peak T (1.690 eV) usually attributed to trion (charged exciton) and lower energy lines (1.65–1.68 eV) usually attributed to localized excitons, in agreement with already published results [26,27,41]. Please note that we did not observe any signature of the T transition in reflectivity, indicating a small oscillator strength and suggesting that the ML is actually in the neutral regime as recently confirmed in charge tunable encapsulated samples [42]. For this geometry where the light is polarized in the ML plane [43], the detected neutral exciton luminescence X^0 corresponds to the radiative recombination involving both Γ_{11} conduction band (CB) and Γ_7 valence band (VB) in the valley $\boldsymbol{K}_+$ and Γ_{12} conduction band and Γ_8 valence band in the valley $\boldsymbol{K}_-$; see the green arrows in Fig. 1(e). Both transitions conserve the spin. In contrast the transitions in the $\boldsymbol{K}_+$ valley between the Γ_9 CB and Γ_7 VB with opposite spins (Γ_{10} CB and Γ_8 VB in the $\boldsymbol{K}_-$ valley) are optically forbidden for the in-plane polarized light. The energy difference between the corresponding dark exciton and the bright X^0 depends both on the spin-orbit splitting in the conduction band $\Delta_{\mathrm{SO}}^{\mathrm{CB}}$ and the short-range part of the electron-hole exchange interaction, where $\Delta_{\mathrm{SO}}^{\mathrm{CB}}$ is the energy difference between Γ_9 (Γ_{10}) CB and Γ_{11} (Γ_{12}) in valley $\boldsymbol{K}_+$ ($\boldsymbol{K}_-$). The calculations predict values $\Delta_{\mathrm{bright-dark}}$ of a few tens of meV for WSe_2 ML [23,48].

We present now the key results associated to the measurements from the edge of the sample [see Fig. 1(b)]. The great advantage of this geometry is that it is suitable for measuring the interaction of the 2D material with light for both polarization directions, parallel to the plane of the ML, x polarized, as in Fig. 1(c) or perpendicular to it, z polarized.

The optical selection rules, which depend intimately on the band structure of the ML and the exciton symmetry, can thus be revealed. In Fig. 1(d) the PL spectra of the WSe_2 ML for both in-plane (x) and perpendicular (z) to the plane polarization are displayed. As expected the in-plane polarized PL spectrum (green line) is very similar to the normal incidence excitation or detection geometry shown in Fig. 1(c). As the polarization of the detected luminescence is identical, the same optical selection rules apply and we observe the lines associated to neutral excitons (X^0), T, and localized excitons. The detection energies of the lines are identical for both geometries but we note a larger broadening for excitation or detection from the sample edge. This might be the result of a longer interaction length in the 2D material or enhanced scattering rates due to in-plane excitation. Remarkably a new line labeled X^D shows up in addition to the previous ones when the luminescence polarized perpendicular to the ML is detected [red line in Fig. 1(d)]. In agreement with the selection rules detailed below, this peak corresponds to the radiative recombination of excitons involving the transitions between the bottom Γ_9 (Γ_{10}) CB and topmost Γ_7 (Γ_8) VB in the valley $\boldsymbol{K}_+$ ($\boldsymbol{K}_-$). We recall that these transitions are optically forbidden (dark excitons) for in-plane polarized light, in agreement with the x-polarized spectrum in Fig. 1(c). As a consequence the energy difference between X^0 and X^D in Fig. 1(d) is a direct measurement of the bright-dark exciton splitting. We find $\Delta_{\text{bright-dark}} = 40 \pm 1$ meV in WSe_2. Note that the absence of any signature of dark trions is consistent with a ML being in the neutral regime. Figure 2(a) presents the result of the same experiment performed on WS_2 ML at $T = 13$ K. Again when the luminescence polarized perpendicular to the ML is detected, a new line (X^D) shows up and we measure a bright-dark exciton splitting energy of 55 ± 2 meV. These accurate measurements are a key element to improve the parametrization of *ab initio* calculations of the band structure [23].

Finally we perform the same investigation for a $MoSe_2$ ML both at $T = 13$ and 300 K. No spectral signature of the X^D line is observed in $MoSe_2$ ML in Fig. 2(b) at low temperature and in Fig. S4 of Supplemental Material [44] at higher temperature. This behavior is compatible with our current understanding of the $MoSe_2$ ML band structure. Though the exact value of $\Delta_{\text{bright-dark}}$ is still unknown, both theoretical and experimental investigations predict that the dark exciton lies at higher energy compared to the bright one (in contrast to WSe_2 and WS_2 ML) [25–28]. The main reason is the change of sign of the spin-orbit splitting in the conduction band between these different materials [29]. Very recent investigations based on the coupling of the excitons to transverse high magnetic fields (tens of teslas) [49,50], or surface plasmon polaritons [51], inferred similar bright-dark exciton splitting energies. We emphasize that our measurements are based on the intrinsic properties of the MLs and do not require any external perturbation in addition to the light. For the sake of completeness we have

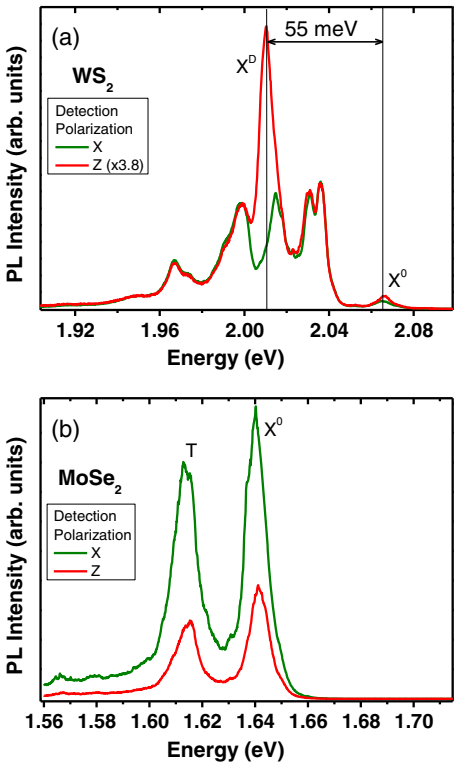

FIG. 2. Detection of the PL from the edge of the sample. The PL spectrum at $T = 13$ K for (a) $h - BN/WS_2$ ML/h-BN and (b) $h - BN/MoSe_2$ ML/h-BN; the polarization of the excitation or detected light is in the ML plane (x direction), green line, or perpendicular to it (z direction), red line.

also investigated the dependence of the PL spectra detected from the edge of the sample as a function of the polarization of the excitation laser propagating along the ML plane. In the previous experiments, Figs. 1 and 2, the laser was polarized in the ML plane along the x axis. When the excitation laser is z polarized, we observe a decrease of the PL intensity of both X^0 and X^D lines (see Fig. S2 in [44]). This could be the consequence of the smaller absorption for the z-polarized transition compared to the x-polarized one. However, quantitative conclusions cannot be drawn from those measurements since the precise selection rules for nonresonant laser excitation are difficult to determine.

The conclusions drawn from the experimental results are confirmed by the group theory analysis of the selection rules. Let us recall that the orbital Bloch functions of the valence band in $\boldsymbol{K}_+$ and $\boldsymbol{K}_-$ transform according to the same scalar representation Γ_1 (notations of Ref. [52]) of the C_{3h} point group relevant at the $\boldsymbol{K}_\pm$ points. The conduction band orbital Bloch functions transform according to Γ_2 and Γ_3, respectively. As a result, the spinor representations for the valence band are Γ_7 ($\uparrow$) and Γ_8 ($\downarrow$), while for the conduction band, Fig. 1(e), they are

$$\Gamma_2 \times \Gamma_7 = \Gamma_{11}, \qquad \Gamma_2 \times \Gamma_8 = \Gamma_9, \tag{1a}$$

$$\Gamma_3 \times \Gamma_7 = \Gamma_{10}, \qquad \Gamma_3 \times \Gamma_8 = \Gamma_{12}. \tag{1b}$$

Interband optical excitation gives rise to the electron-hole pairs bound into excitons by the Coulomb interaction. The excitonic states with $1s$ envelope function detected in our experiments transform according to the representations $\Gamma_X = \Gamma_c \times \Gamma_v^*$, where Γ_c is the representation of the conduction band state and Γ_v is the representation of the empty valence band state. Note that the hole state is the time reversal of the unoccupied valence band state; therefore, the conjugation of Γ_v is needed [53]. The exciton state is optically active in a given polarization if Γ_X contains the irreducible representation according to which the corresponding polarization vector $\boldsymbol{e}$ transforms. As a consequence for the optically active excitons Γ_X must contain $\Gamma_2 + \Gamma_3$, i.e., the in-plane polarization, or Γ_4, z polarization. Hereafter we consider only vertical optical transitions and obtain for possible symmetries of the exciton

$$\Gamma_{12} \times \Gamma_8^* = \Gamma_3, \qquad \Gamma_{11} \times \Gamma_7^* = \Gamma_2 \tag{2a}$$

$$\Gamma_{10} \times \Gamma_8^* = \Gamma_4, \qquad \Gamma_9 \times \Gamma_7^* = \Gamma_4. \tag{2b}$$

The basic functions of Γ_2 and Γ_3 irreducible representations transform as $x \pm iy$, respectively. Hence, Eq. (2a) describes the excitons active in the σ^+ and σ^- polarizations at the normal incidence of radiation; see green arrows in Figs. 1(e) and 1(f). Here the electron spin in the course of the interband transition is conserved and the polarization of the PL is determined by the orbital character of the Bloch functions. By contrast, the transitions involving opposite spins for the conduction and valence band states are forbidden at the normal incidence because they couple with the light of z polarization, i.e., normal to the ML plane. These transitions are depicted by red arrows in Fig. 1(f). This is in agreement with the measurement of the additional line X^D, which is z polarized in Figs. 1(d) and 2(a) for WSe_2 and WS_2 ML, respectively.

A deeper insight into the symmetry of excitonic states can be obtained by considering the irreducible representations of the D_{3h} point group relevant for the overall symmetry of the ML. Such an analysis allows one to study the mixing of excitons in different valleys. The results in Supplemental Material [44] demonstrate that out of two z-polarized states, $\Gamma_{X_1} = \Gamma_{10} \times \Gamma_8^*$ and $\Gamma_{X_2} = \Gamma_9 \times \Gamma_7^*$, one linear combination with equal weights is active in the z polarization and can be attributed to the X^D line, while another one is forbidden.

As these transitions require spin-orbit interaction to induce spin mixing, their oscillator strengths are expected to be much weaker than the one for in-plane polarized light. It can be qualitatively described by taking into account, for example, the interaction of the upper valence bands, Γ_7 and Γ_8, or lower conduction bands, Γ_9 and Γ_{10}, with remote bands with different orbital character and opposite spin orientations; see Supplemental Material [44]. Recent density functional theory calculations performed at the GW level combined with the Bethe-Salpeter equation for excitons predict that the out-of-plane contribution is $\sim 10^3$ times smaller than the in-plane one [23]. Though our experiments clearly evidence both transitions, the measured PL intensities cannot be used for the accurate determination of the relative ratio of the oscillator strengths since the nonresonant excitation results in unknown populations of the exciton states X^0 and X^D. Particularly, the assumption of a thermodynamical equilibrium between the X^0 and X^D is questionable considering the very short radiative lifetime of X^0 [54–56]. Further investigations based, e.g., on absorption or photocurrent measurements performed with strictly resonant excitation are required.

Finally we note in the spectrum shown in the inset of Fig. 1(c), obtained with a microscope objective with a large NA of 0.82, a line visible at the energy X^D (1.68 eV), which is, in principle, forbidden for excitation or detection at normal incidence with respect to the ML. The observation of this line is, actually, not surprising: First it can have a purely geometric origin. As we use a microscope objective with high NA, the electric field vector at the focal tail has a significant component along the z axis that enables excitation or detection of the X^D transition even at the normal incidence. The percentage of the z mode to the total intensity was estimated to be $\sim 9\%$ in a similar study performed in GaAs quantum wells [57]. Second, a lowering of the symmetry of the 2D crystal due to local strain or ripples can induce a small mixing between bright and dark excitons, yielding the observation of the X^D component even for normal incidence [58]. To elucidate the origin of the peak at 1.68 eV seen in the inset of Fig. 1(c) we note that by detecting only the central part of the PL spot for normal incidence excitation or detection, the X^D line totally vanishes confirming that the z component is located of axis only; see Fig. S5 of Supplemental Material [44]. This demonstrates that the X^D line observed in the inset of Fig. 1(c) is simply linked to the geometry of the experiment based on a microscope objective with a large numerical aperture. Note that similar arguments on geometry can be applied to edge illumination and collection of the PL. The laser beam inevitably hits the monolayer surface at very acute angles. This small PL contribution through the front surface can also be part of the signal detected in the experimental geometry of Fig. 1(b).

In addition to their importance for the knowledge of the band structure and excitonic properties in TMDC MLs, these experiments pave the way to the investigation of waveguides heterostructures and devices based on 2D materials.

We acknowledge ERC Grant No. 306719, ITN Spin-NANO Marie Sklodowska-Curie Grant No. 676 108, ANR MoS2ValleyControl, and Programme Investissements d Avenir Grant No. ANR-11-IDEX-0002-02, reference ANR-10- LABX-0037-NEXT for financial support, and Laboratoire International Associe

Grant No. ILNACS CNRS-Ioffe. X. M. also acknowledges the Institut Universitaire de France. K. W. and T. T. acknowledge support from the Elemental Strategy Initiative conducted by the MEXT, Japan and JSPS KAKENHI Grants No. JP26248061, No. JP15K21722, and No. JP25106006. M. M. G. is grateful to the RFBR (17-02-00383 and 17-52-16020), Dynasty Foundation and RF President Grant No. MD-1555.2017.2 for partial support.

[1] S. Z. Butler, S. M. Hollen, L. Cao, Y. Cui, J. A. Gupta, H. R. Gutiérrez, T. F. Heinz, S. S. Hong, J. Huang, A. F. Ismach, E. Johnston-Halperin, M. Kuno, V. V. Plashnitsa, R. D. Robinson, R. S. Ruoff, S. Salahuddin, J. Shan, L. Shi, M. G. Spencer, M. Terrones, W. Windl, and J. E. Goldberger, Progress, challenges, and opportunities in two-dimensional materials beyond graphene, ACS Nano **7**, 2898 (2013).

[2] A. K. Geim and I. V. Grigorieva, Van der Waals heterostructures, Nature (London) **499**, 419 (2013).

[3] K. F. Mak, C. Lee, J. Hone, J. Shan, and T. F. Heinz, Atomically Thin MoS_2: A New Direct-Gap Semiconductor, Phys. Rev. Lett. **105**, 136805 (2010).

[4] A. Splendiani, L. Sun, Y. Zhang, T. Li, J. Kim, C.-Y. Chim, G. Galli, and F. Wang, Emerging photoluminescence in monolayer MoS_2, Nano Lett. **10**, 1271 (2010).

[5] Q. H. Wang, K. Kalantar-Zadeh, A. Kis, J. N. Coleman, and M. S. Strano, Electronics and optoelectronics of two-dimensional transition metal dichalcogenides, Nat. Nanotechnol. **7**, 699 (2012).

[6] K. He, N. Kumar, L. Zhao, Z. Wang, K. F. Mak, H. Zhao, and J. Shan, Tightly Bound Excitons in Monolayer WSe_2, Phys. Rev. Lett. **113**, 026803 (2014).

[7] M. M. Ugeda, A. J. Bradley, S.-F. Shi, F. H. da Jornada, Y. Zhang, D. Y. Qiu, S.-K. Mo, Z. Hussain, Z.-X. Shen, F. Wang, S. G. Louie, and M. F. Crommie, Observation of giant band-gap renormalization and excitonic effects in a monolayer transition metal dichalcogenide semiconductor, Nat. Mater. **13**, 1091 (2014).

[8] A. Chernikov, T. C. Berkelbach, H. M. Hill, A. Rigosi, Y. Li, O. Burak Aslan, D. R. Reichman, M. S. Hybertsen, and T. F. Heinz, Exciton Binding Energy and Nonhydrogenic Rydberg Series in Monolayer WS_2, Phys. Rev. Lett. **113**, 076802 (2014).

[9] Z. Ye, T. Cao, K. O'Brien, H. Zhu, X. Yin, Y. Wang, S. G. Louie, and X. Zhang, Probing excitonic dark states in single-layer tungsten disulfide, Nature (London) **513**, 214 (2014).

[10] D. Y. Qiu, F. H. da Jornada, and S. G. Louie, Optical Spectrum of MoS_2: Many-Body Effects and Diversity of Exciton States, Phys. Rev. Lett. **111**, 216805 (2013).

[11] A. Ramasubramaniam, Large excitonic effects in monolayers of molybdenum and tungsten dichalcogenides, Phys. Rev. B **86**, 115409 (2012).

[12] G. Wang, X. Marie, I. Gerber, T. Amand, D. Lagarde, L. Bouet, M. Vidal, A. Balocchi, and B. Urbaszek, Giant Enhancement of the Optical Second-Harmonic Emission of WSe_2 Monolayers by Laser Excitation at Exciton resonances, Phys. Rev. Lett. **114**, 097403 (2015).

[13] D. Xiao, G.-B. Liu, W. Feng, X. Xu, and W. Yao, Coupled Spin and Valley Physics in Monolayers of MoS_2 and other Group-VI Dichalcogenides, Phys. Rev. Lett. **108**, 196802 (2012).

[14] G. Sallen, L. Bouet, X. Marie, G. Wang, C. R. Zhu, W. P. Han, Y. Lu, P. H. Tan, T. Amand, B. L. Liu, and B. Urbaszek, Robust optical emission polarization in MoS_2 monolayers through selective valley excitation, Phys. Rev. B **86**, 081301 (2012).

[15] K. F. Mak, K. He, J. Shan, and T. F. Heinz, Control of valley polarization in monolayer MoS_2 by optical helicity, Nat. Nanotechnol. **7**, 494 (2012).

[16] G. Kioseoglou, A. T. Hanbicki, M. Currie, A. L. Friedman, D. Gunlycke, and B. T. Jonker, Valley polarization and intervalley scattering in monolayer MoS_2, Appl. Phys. Lett. **101**, 221907 (2012).

[17] T. Cao, G. Wang, W. Han, H. Ye, C. Zhu, J. Shi, Q. Niu, P. Tan, E. Wang, B. Liu, and J. Feng, Valley-selective circular dichroism in MoS_2, Nat. Commun. **3**, 887 (2012).

[18] A. M. Jones, H. Yu, N. J. Ghimire, S. Wu, G. Aivazian, J. S. Ross, B. Zhao, J. Yan, David G. Mandrus, D. Xiao, W. Yao, and X. Xu, Optical generation of excitonic valley coherence in monolayer WSe_2, Nat. Nanotechnol. **8**, 634 (2013).

[19] L. Yang, N. A. Sinitsyn, W. Chen, J. Yuan, J. Zhang, J. Lou, and S. A. Crooker, Long-lived nanosecond spin relaxation and spin coherence of electrons in monolayer MoS_2 and WS_2, Nat. Phys. **11**, 830 (2015).

[20] J. S. Weiner, D. S. Chemla, D. A. B. Miller, H. A. Haus, A. C. Gossard, W. Wiegmann, and C. A. Burrus, Highly anisotropic optical properties of single quantum well waveguides, Appl. Phys. Lett. **47**, 664 (1985).

[21] J.-Y. Marzin, M. N. Charasse, and B. Sermage, Optical investigation of a new type of valence-band configuration in strained superlattices, Phys. Rev. B **31**, 8298 (1985).

[22] M. M. Glazov, T. Amand, X. Marie, D. Lagarde, L. Bouet, and B. Urbaszek, Exciton fine structure and spin decoherence in monolayers of transition metal dichalcogenides, Phys. Rev. B **89**, 201302 (2014).

[23] J. P. Echeverry, B. Urbaszek, T. Amand, X. Marie, and I. C. Gerber, Splitting between bright and dark excitons in transition metal dichalcogenide monolayers, Phys. Rev. B **93**, 121107 (2016).

[24] A. O. Slobodeniuk and D. M. Basko, Spin-flip processes and radiative decay of dark intravalley excitons in transition metal dichalcogenide monolayers, 2D Mater. **3**, 035009 (2016).

[25] X.-X. Zhang, Y. You, S. Y. F. Zhao, and T. F. Heinz, Experimental Evidence for Dark Excitons in Monolayer WSe_2, Phys. Rev. Lett. **115**, 257403 (2015).

[26] G. Wang, C. Robert, A. Suslu, B. Chen, S. Yang, S. Alamdari, I. C. Gerber, T. Amand, X. Marie, S. Tongay, and B. Urbaszek, Spin-orbit engineering in transition metal dichalcogenide alloy monolayers, Nat. Commun. **6**, 10110 (2015).

[27] A. Arora, M. Koperski, K. Nogajewski, J. Marcus, C. Faugeras, and M. Potemski, Excitonic resonances in thin films of WSe_2: From monolayer to bulk material, Nanoscale **7**, 10421 (2015).

[28] F. Withers, O. Del Pozo-Zamudio, S. Schwarz, S. Dufferwiel, P. M. Walker, T. Godde, A. P. Rooney, A. Gholinia, C. R. Woods, P. Blake, S. J. Haigh, K. Watanabe, T. Taniguchi, I. L.

Aleiner, A. K. Geim, V. I. Fal'ko, A. I. Tartakovskii, and K. S. Novoselov, WSe_2 light-emitting tunneling transistors with enhanced brightness at room temperature, Nano Lett. **15**, 8223 (2015).

[29] K. Kośmider, J. W. González, and J. Fernández-Rossier, Large spin splitting in the conduction band of transition metal dichalcogenide monolayers, Phys. Rev. B **88**, 245436 (2013).

[30] A. Kormanyos, G. Burkard, M. Gmitra, J. Fabian, V. Zolyomi, N. D. Drummond, and V. Fal'ko, k.p theory for two-dimensional transition metal dichalcogenide semiconductors, 2D Mater. **2**, 022001 (2015).

[31] H. Dery and Y. Song, Polarization analysis of excitons in monolayer and bilayer transition-metal dichalcogenides, Phys. Rev. B **92**, 125431 (2015).

[32] Z. Wang, L. Zhao, K. F. Mak, and J. Shan, Probing the spin-polarized electronic band structure in monolayer transition metal dichalcogenides by optical spectroscopy, Nano Lett. **17**, 740 (2017).

[33] O. A. Ajayi, J. V. Ardelean, G. D. Shepard, J. Wang, A. Antony, T. Taniguchi, K. Watanabe, T. F. Heinz, S. Strauf, X.-Y. Zhu, and J. C. Hone, Approaching the Intrinsic Photoluminescence Linewidth in Transition Metal Dichalcogenide Monolayers, arXiv:1702.05857.

[34] F. Cadiz, E. Courtade, C. Robert, G. Wang, Y. Shen, H. Cai, T. Taniguchi, K. Watanabe, H. Carrere, D. Lagarde, M. Manca, T. Amand, P. Renucci, S. Tongay, X. Marie, and B. Urbaszek, Excitonic Linewidth Approaching the Homogeneous Limit in MoS_2-Based van der Waals Heterostructures: Accessing Spin-Valley Dynamics, Phys. Rev. X **7**, 021026 (2017).

[35] M. Manca, M. M. Glazov, C. Robert, F. Cadiz, T. Taniguchi, K. Watanabe, E. Courtade, T. Amand, P. Renucci, X. Marie, G. Wang, and B. Urbaszek, Enabling valley selective exciton scattering in monolayer WSe_2 through up conversion, Nat. Commun. **8**, 14927 (2017).

[36] T. Taniguchi and K. Watanabe, Synthesis of high-purity boron nitride single crystals under high pressure by using ba-bn solvent, J. Cryst. Growth **303**, 525 (2007).

[37] G. Wang, L. Bouet, D. Lagarde, M. Vidal, A. Balocchi, T. Amand, X. Marie, and B. Urbaszek, Valley dynamics probed through charged and neutral exciton emission in monolayer WSe_2, Phys. Rev. B **90**, 075413 (2014).

[38] For the measurements from the edge of the sample, the ratio between the focused laser spot diameter and the thickness of the ML is smaller than 1000. Though challenging from the point of view of the required alignment accuracy this experiment can be successful as shown below thanks to (i) the very large absorption coefficient of the TMD ML for in-plane polarized light [39] and (ii) the detection efficiency of our setup, designed for studies of single photon emitters [40].

[39] Y. Li, A. Chernikov, X. Zhang, A. Rigosi, H. M. Hill, A. M. van der Zande, D. A. Chenet, E.-M. Shih, J. Hone, and T. F. Heinz, Measurement of the optical dielectric function of monolayer transition-metal dichalcogenides: MoS_2, $MoSe_2$, WS_2, and WSe_2, Phys. Rev. B **90**, 205422 (2014).

[40] T. Belhadj, C.-M. Simon, T. Amand, P. Renucci, B. Chatel, O. Krebs, A. Lemaître, P. Voisin, X. Marie, and B. Urbaszek, Controlling the Polarization Eigenstate of a Quantum Dot Exciton with Light, Phys. Rev. Lett. **103**, 086601 (2009).

[41] A. M. Jones, H. Yu, J. R. Schaibley, J. Yan, D. G. Mandrus, T. Taniguchi, K. Watanabe, H. Dery, W. Yao, and X. Xu, Excitonic luminescence up conversion in a two-dimensional semiconductor, Nat. Phys. **12**, 323 (2016).

[42] E. Courtade, M. Semina, M. Manca, M. M. Glazov, C. Robert, F. Cadiz, G. Wang, T. Taniguchi, K. Watanabe, M. Pierre, W. Escoffier, E. L. Ivchenko, P. Renucci, X. Marie, T. Amand, and B. Urbaszek, Charged excitons in monolayer WSe_2: Experiment and theory, arXiv:1705.02110.

[43] Note that for the experiment in Fig. 1(c) a low NA microscope objective was used, to probe selection rules normal to the ML plane. In the inset of the same figure we show the same experiment using a high NA objective, for which we confirm the main emission lines X^0 and T. In addition we see a sharp transition about 40 meV below X^0, which we show to be related to the electric field vector having a non-negligible out-of-plane (z) component; see Fig. S5 of Supplemental Material [44].

[44] See Supplemental Material at http://link.aps.org/supplemental/10.1103/PhysRevLett.119.047401, which includes Refs. [45–47] and contains additional experimental data and detailed group theory and effective Hamiltonian analysis.

[45] G. Wang, L. Bouet, M. M. Glazov, T. Amand, E. L. Ivchenko, E. Palleau, X. Marie, and B. Urbaszek, Magneto-optics in transition metal diselenide monolayers, 2D Mater. **2**, 034002 (2015).

[46] G. E. Pikus, V. A. Maruschak, and A. N. Titkov, Spin splitting of energy bands and spin relaxation of carriers in cubic III-V crystals, Sov. Phys. Semicond. **22**, 115 (1988).

[47] M. M. Glazov, L. E. Golub, G. Wang, X. Marie, T. Amand, and B. Urbaszek, Intrinsic exciton-state mixing and nonlinear optical properties in transition metal dichalcogenide monolayers, Phys. Rev. B **95**, 035311 (2017).

[48] D. Y. Qiu, T. Cao, and S. G. Louie, Nonanalyticity, Valley Quantum Phases, and Lightlike Exciton Dispersion in Monolayer Transition Metal Dichalcogenides: Theory and First-Principles Calculations, Phys. Rev. Lett. **115**, 176801 (2015).

[49] X. Zhang, T. Cao, Z. Lu, Y. Lin, F. Zhan, Y. Wang, Z. Li, J. C. Hone, J. A. Robinson, D. Smirnov, S. G. Louie, and T. F. Heinz, Magnetic brightening and control of dark excitons in monolayer wse 2, arXiv:1612.03558.

[50] M. R. Molas, C. Faugeras, A. O. Slobodeniuk, K. Nogajewski, M. Bartos, D. M. Basko, and M. Potemski, Brightening of dark excitons in monolayers of semiconducting transition metal dichalcogenides, 2D Mater. **4**, 021003 (2017).

[51] Y. Zhou, G. Scuri, D. S. Wild, A. A. High, A. Dibos, L. A. Jauregui, C. Shu, K. de Greve, K. Pistunova, A. Joe, T. Taniguchi, K. Watanabe, P. Kim, M. D. Lukin, and H. Park, Probing dark excitons in atomically thin semiconductors via near-field coupling to surface plasmon polaritons, arXiv:1701.05938.

[52] G. F. Koster, J. O. Dimmock, G. Wheeler, and R. G. Satz, *Properties of Thirty-Two Point Groups* (M.I.T. Press, Cambridge, 1963).

[53] M. M. Glazov, E. L. Ivchenko, G. Wang, T. Amand, X. Marie, B. Urbaszek, and B. L. Liu, Spin and valley

dynamics of excitons in transition metal dichalcogenide monolayers, Phys. Status Solidi (b) **252**, 2349 (2015).

[54] T. Korn, S. Heydrich, M. Hirmer, J. Schmutzler, and C. Schüller, Low-temperature photocarrier dynamics in monolayer MoS_2, Appl. Phys. Lett. **99**, 102109 (2011).

[55] D. Lagarde, L. Bouet, X. Marie, C. R. Zhu, B. L. Liu, T. Amand, P. H. Tan, and B. Urbaszek, Carrier and Polarization Dynamics in Monolayer MoS_2, Phys. Rev. Lett. **112**, 047401 (2014).

[56] C. Robert, D. Lagarde, F. Cadiz, G. Wang, B. Lassagne, T. Amand, A. Balocchi, P. Renucci, S. Tongay, B. Urbaszek, and X. Marie, Exciton radiative lifetime in transition metal dichalcogenide monolayers, Phys. Rev. B **93**, 205423 (2016).

[57] M. Schardt, A. Winkler, G. Rurimo, M. Hanson, D. Driscoll, S. Quabis, S. Malzer, G. Leuchs, G. H. Döhler, and A. C. Gossard, TE- and TM-polarization-resolved spectroscopy on quantum wells under normal incidence, Physica **32E**, 241 (2006).

[58] M. Bayer, G. Ortner, O. Stern, A. Kuther, A. A. Gorbunov, A. Forchel, P. Hawrylak, S. Fafard, K. Hinzer, T. L. Reinecke, S. N. Walck, J. P. Reithmaier, F. Klopf, and F. Schäfer, Fine structure of neutral and charged excitons in self-assembled in(ga)as/(al)gaas quantum dots, Phys. Rev. B **65**, 195315 (2002).